

Characterisation of the Basel 1 enhanced geothermal system

Markus O. Häring^a, Ulrich Schanz^{a,*},
Florentin Ladner^a, Ben C. Dyer^b

^a *Geothermal Explorers Ltd., Pratteln, Switzerland*

^b *Semore Seismic, Cornwall, UK*

Received 16 June 2008; accepted 17 June 2008

Available online 26 July 2008

Abstract

This paper describes the steps that have been undertaken to create an enhanced geothermal system (EGS) at the Deep Heat Mining Project in Basel, Switzerland. Preliminary results from drilling, logging, hydraulic testing and stimulating the Basel 1 well are summarized. The project was suspended following the occurrence of several ‘felt’ microseismic events. Because such events may be an inherent risk with current methods of reservoir stimulation, the paper analyses the possible mechanisms of hydraulically induced shearing processes and suggests methods by which the risk may be reduced. The observations are integrated into a model of the geothermal reservoir where aspects of both the reservoir development and the driving mechanism for the perceptible induced seismic events are considered.

© 2008 Elsevier Ltd. All rights reserved.

Keywords: Geothermal; Enhanced geothermal systems; Deep Heat Mining Basel; Stress field; Hydraulic stimulation; Induced seismicity; Fracture zones

1. Introduction

The generation of an efficient hydraulic subsurface heat exchanger system is crucial for economic production of electricity and heat from an enhanced geothermal system (EGS). The circulation of water at sufficiently low flow impedances through natural discontinuities typically requires hydraulic stimulation to improve the hydraulic properties of the naturally fractured hot rock mass.

* Corresponding author. Tel.: +41 61 821 60 40; fax: +41 61 821 60 44.

E-mail address: ulrich.schanz@geothermal.ch (U. Schanz).

The Deep Heat Mining (DHM) Project was initiated in order to develop a geothermal cogeneration plant from an EGS in the city of Basel, Switzerland. For this purpose a microseismic monitoring array was put into operation in February 2006 and the well Basel 1 was drilled between May and October 2006 to a total depth¹ of 5 km through 2.4 km of sedimentary rocks and 2.6 km of granitic basement. After an extensive logging and testing phase, the granite in the open hole below 4629 m depth was hydraulically stimulated to enhance the permeability.

The stimulation operation was planned to take 21 days. However, high rates of microseismic activity built up during the first 6 days of fluid injection with event magnitudes of up to M_L 2.6. In view of this, it was decided to stop the injection. The decision adhered to a pre-defined seismic response procedure approved by the local authorities, which specified the measures to be taken at increased levels of seismic activity (see Section 3.2). After shutting in the well for about 5 h, a seismic event of M_L 3.4 occurred during preparations for bleeding off the well to hydrostatic conditions. Over the following 56 days, three aftershocks of $M_L > 3$ were recorded. At present the project is suspended but not abandoned pending an independent risk analysis and identification of acceptable ways of reservoir enhancement.

Below we summarize the preliminary results from drilling, logging, testing and stimulating the Basel 1 well and suggest a reservoir model where some aspects of both the reservoir development and the driving mechanism for the perceptible induced seismic events are described.

1.1. Tectonics and seismicity

The city of Basel is located in northwestern Switzerland at the south-eastern margin of the Upper Rhine Graben (Fig. 1), which is part of the European Cenozoic rift system, one of the major intracontinental tectonic features in Western Europe (Laubscher, 2001; Dèzes et al., 2004). The southernmost Upper Rhine Graben, including the Basel region, is situated in the junction area between this pre-existing Eo-Oligocene rift and the northern rim of the younger Jura fold and thrust belt that formed in Latest Miocene to recent times.

The fault pattern in the Upper Rhine Graben at this location consists of three sets of faults striking NNE, ENE and NW that relate to the rift/graben structure, the Rhine-Bresse transfer zone and the Variscian orogeny, respectively. These basement fracture zones are prone to present-day activation by neotectonic activity (Ustazewski and Schmid, 2007).

The seismicity in the Upper Rhine Graben can be characterized by frequent minor seismicity and occasional destructive seismicity. The activity has been more pronounced in the southern part, where the graben intersects the Jura folds. The largest known historical earthquake in central-northern Europe, with an estimated M_L of 6.5 to 6.9, occurred in Basel in 1356 (Giardini et al., 2004). In recent times most of the natural earthquakes in the Basel area have been small to moderate events. Within a 10-km radius around the city of Basel, 15 events with $M_L \geq 2$ and 10 events with $1 \leq M_L \leq 2$ have occurred since 1975.

1.2. Regional stress field

The stress field in the Upper Rhine Graben area, inferred from fault plane solutions of natural seismic events in the crystalline basement, is characterised by a strike-slip regime with a NW-orientation of maximum horizontal stress (S_{Hmax}) (Plenefisch and Bonjer, 1997; Deichmann et

¹ All depths are depths below ground surface.

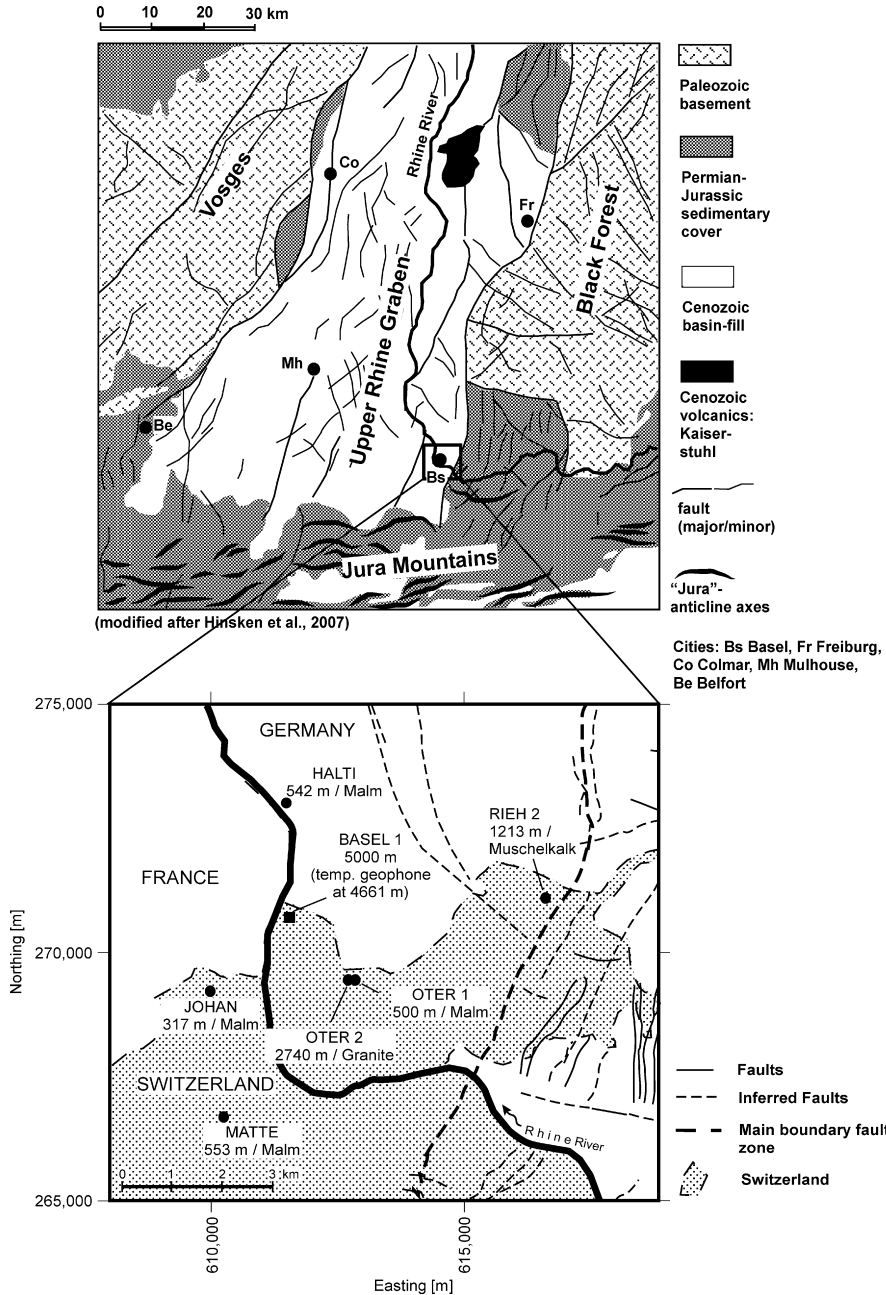


Fig. 1. Schematic geological and tectonic map of the southern Upper Rhine Graben. Lower panel: microseismic network; seismic stations marked by black circles. After the name of each of the stations the depth and the formation where the geophone has been installed are given. The square corresponds to the location of the deep geothermal well Basel 1 where a deep geophone sensor was temporarily deployed to calibrate the seismic velocity model; see Dyer et al. (2008) for more details. [See Ref. Hirsken et al., 2007]

al., 2000; Kastrop et al., 2004). These results are consistent with the large-scale pattern of stress in Europe, which appears to be dominated by NW-oriented compression (Reinecker et al., 2005).

2. Geological, geomechanical and hydraulic characterization of the Basel 1 reservoir

2.1. Well geology and reservoir temperature

The well Basel 1 passed through 2411 m of Quaternary, Tertiary, Mesozoic and Permian sediments and approximately 100 m of red Permian siltstone and weathered granite before entering crystalline basement at 2507 m depth (Fig. 2). This basement corresponds to the southern continuation of the Black Forest massif and is exclusively comprised of plutonic rocks; no metamorphic rocks were observed in Basel 1.

The primary basement rock types include granitoid rocks (>99%), aplite and lamprophyre. The granitoid plutonic rocks are mainly hornblende-bearing biotite granite, hornblende–biotite monzogranite and monzonite. The major rock-forming minerals are plagioclase, K-feldspar, quartz, hornblende, biotite and titanite with accessory minerals apatite, zircon, allanite and magnetite. In the deeper part of the borehole the rocks are more basic (hornblende–biotite-rich) and quartz-poor. Geochemical parameters indicate that the Basel 1 monzogranites are I-type granitoids, meaning that their parental magma formed by melting of older igneous rocks (Käser et al., 2007).

The crystalline basement was logged with an acoustic borehole imager from 2557 m to 5000 m depth in order to determine the frequency and orientation of natural and induced fractures (tensile fractures and borehole breakouts). A total of 984 natural fractures were detected. In the upper part of the basement the fracture density has a maximum value of 0.95 per meter. In the lower part of the well, including the open hole section at 4629–5000 m, the fracture density decreases to 0.2–0.3 per meter. The dominant natural fracture set strikes NW-SE to NNW-SSE, with steep dips exceeding 60° (Fig. 3).

Additionally, in the open hole section two major cataclastic fracture zones were identified at 4700 m and 4835 m. Geochemical analyses of drill cuttings show that both zones are highly affected by argillic alteration (illite–muscovite and low fractions of hydro-biotite and mixed layers smectite–illite) and significant amounts of anhydrite (Käser et al., 2007). Unfortunately the orientation of these two fracture zones could not be determined due to highly oversized borehole diameters making a proper analysis impossible with the acoustic borehole imager.

Temperature logs were acquired shortly after reaching the final depth when the reservoir temperature was still disturbed due to cooling effects of the drilling process. Different extrapolation methods (Roux et al., 1980; Ascencio et al., 2006) estimated a reservoir temperature of 190 °C at 5000 m depth.

2.2. Stress orientation

The orientation of the principal stresses was deduced from the acoustic borehole imager log in the crystalline basement section (2600–5000 m) of Basel 1. The well is near-vertical, so borehole breakouts indicate the azimuth of the minimum horizontal stress (S_{Hmin}). Drilling-induced tensile fractures are oriented parallel to the maximum horizontal stress (S_{Hmax}). The analysis of these features shows that S_{Hmin} is oriented along an azimuth of $54 \pm 14^\circ$ (Fig. 3) and the azimuth of S_{Hmax} strikes $144 \pm 14^\circ$ (Valley and Evans, 2006). These orientations are in agreement with previous estimates of the direction of S_{Hmax} of $140 \pm 16^\circ$ in the adjacent reconnaissance well OTER 2, drilled in 2001 to a depth of 2755 m (Fig. 1).

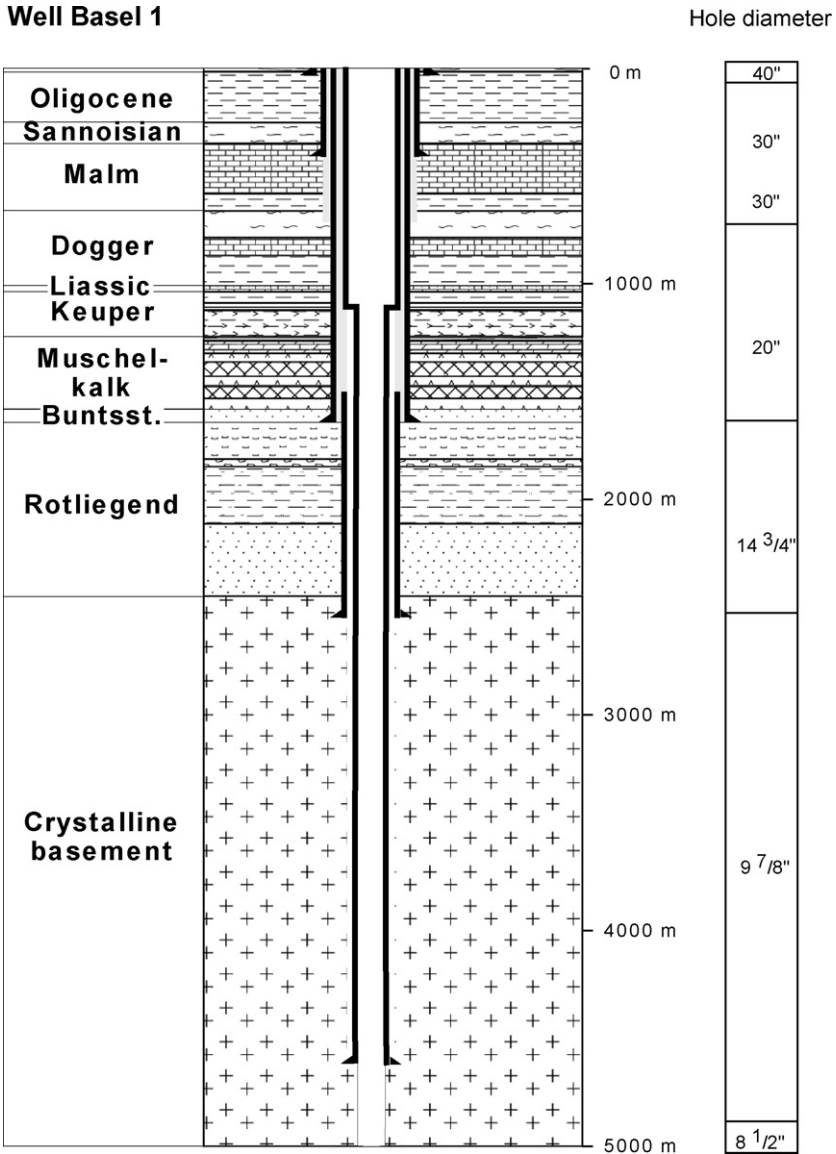


Fig. 2. Well Basel 1: Geological log and well completion. The open hole section extends from 4629 m to 5000 m depth.

2.3. Stress magnitudes

Due to the fact that no hydrofracturing tests were conducted in Basel 1, quantitative information on the magnitude of the stresses remains uncertain. However, constraints on their magnitudes were obtained by combining results from different methods.

In the case of the Basel 1 well a basic constraint is given by the relative stress magnitudes defining a strike-slip regime: $S_{Hmax} > S_V > S_{Hmin}$ ($S_1 = S_{Hmax}$; $S_2 = S_V$; $S_3 = S_{Hmin}$).

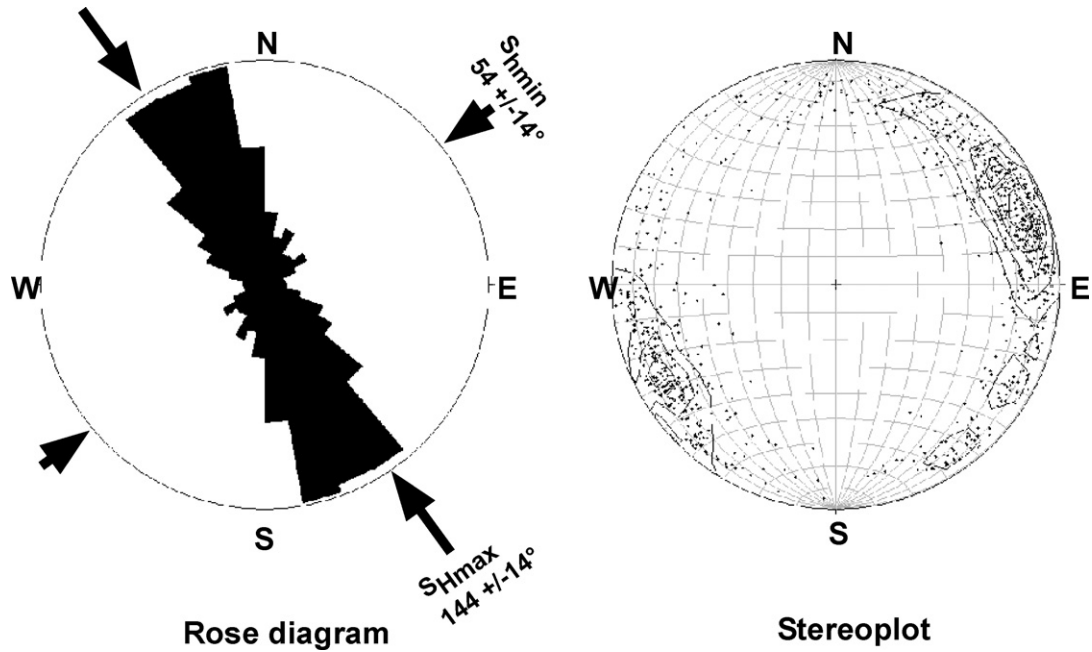


Fig. 3. Left: Rose diagram showing the dominant strikes of natural fractures in the crystalline basement. Arrows indicate the directions of S_{Hmax} from drilling-induced tension fractures and of S_{Hmin} from borehole breakouts. Right: Stereoplot diagram (lower hemisphere equal-area projection) showing the poles for natural planar structures in the crystalline basement.

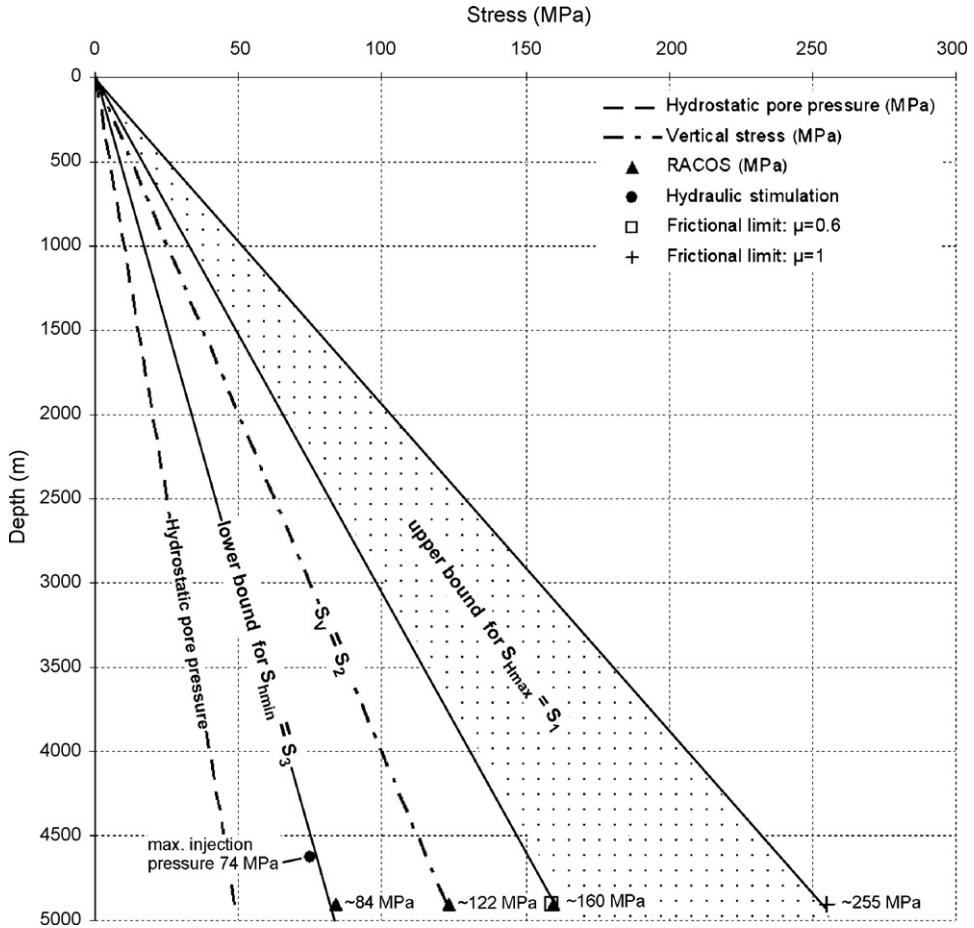


Fig. 4. Constraints on S_{Hmin} and S_{Hmax} in well Basel 1 deduced from hydraulic data, RACOS® (Braun, 2007) and the concept of in situ stress limitations (Zoback, 2007). S_V was calculated by the integration of wireline density logs.

The vertical stress S_V , which represents the overburden, was calculated by integration of the density log acquired in the sedimentary section of nearby well OTER 2 (Fig. 1) and the density log from the crystalline basement of Basel 1. The linear interpolation of these data yields

$$S_V = 0.0249z \tag{1}$$

where S_V is the vertical stress (in MPa) and z is the depth (in meters).

Estimates of the minimum and maximum horizontal stresses were determined using RACOS® (Rock Anisotropy Characterization on Samples; Braun, 2007). The principles of the method are the same as those for differential strain-curve analysis (DSCA) (Charlez, 1997) except that P- and S-wave propagations within the core sample are measured instead of the strain. Although RACOS® is regarded as suitable for stress estimations especially at great depth (Ljunggren et al., 2003), the results represent approximate stress estimations and should be treated with caution. The method was applied in Basel 1 to a core sample from 4911 m depth and the results are shown in Fig. 4. Due to the uncertainty of these results other

techniques were considered in order to constrain the stress magnitudes in the Basel 1 well.

A lower bound constraint on the magnitude of S_{hmin} is provided by the hydraulic stimulation. No pressure-limiting behaviour was observed, suggesting that “formation fracturing” did not occur at the casing shoe (Fig. 5). Thus, the maximum injection pressure applied during stimulation did not exceed the magnitude of S_{hmin} . Consequently the magnitude of S_{hmin} is assumed to be higher than the maximum pressure (74 MPa downhole pressure) reached during stimulation (Fig. 4).

An upper bound constraint on the magnitude of S_{Hmax} is provided by using the concept of in situ stress limitations from the frictional strength of faults (Zoback, 2007). The limiting ratio of principal stresses that cause frictional sliding on optimally oriented faults is given by

$$\frac{S_{Hmax} - P_P}{S_{hmin} - P_P} \leq [(\mu^2 + 1)^{1/2} + \mu]^2 \quad (2)$$

where S_{Hmax} is the maximum principal stress, S_{hmin} is the minimum principal stress, P_P is the hydrostatic pore pressure, and μ is the friction coefficient. The μ value for faults typically falls in the range $0.6 \leq \mu \leq 1$, which yields estimates for S_{Hmax} between 160 MPa and 255 MPa, respectively (Fig. 4). The estimates for S_{Hmax} obtained by RACOS® and derived for a frictional limit $\mu = 0.6$ match very well. Further, this estimate for S_{Hmax} seems to be supported by analysed fault plane solutions of the induced seismic events (see Section 3.4) showing an almost pure strike-slip fault mechanism. This implies a relative stress magnitude $R = (S_V - S_{Hmax}) / (S_{hmin} - S_{Hmax})$ of about 0.5, which yields an estimate for S_{Hmax} in the order of 160 MPa.

Although there are significant uncertainties in inferring stress magnitudes using the various techniques outlined above, taken together they suggest the upper and lower bounds to S_{Hmax} and S_{hmin} shown in Fig. 4.

2.4. Hydraulic characterization of the undisturbed reservoir

On 23 November 2006, a low-rate, 75-h long injection test was conducted in Basel 1 prior to reservoir stimulation in order to characterize pre-existing hydraulic properties of the reservoir. Before the start of the test the mud in the wellbore was completely replaced with freshwater. After shut in, the wellhead pressure built up to 14.8 bar and was still increasing after more than 18 h.

During the low-rate injection test the flow rate was increased in three steps up to a maximum of only 10 L/min over a period of 16 h. However, the steps were not long enough to reach steady-state conditions. At the end of the test the wellhead pressure had built up to 74 bar. Subsequently, the well was shut-in and the pressure dropped to 26.3 bar over the following 11 h, but did not stabilize. Therefore, the steady-state reservoir pressure lies between 17 bar and 26.3 bar with the wellbore filled with fresh water. Since the stimulation (see Section 2.5) the formation fluid has progressively diluted the injected freshwater as the well has been vented. The outflow is now negligible suggesting that the well is not naturally artesian.

The interpretation of the hydraulic data set was performed using “log–log diagnostic plots”. Under the assumption of radial flow conditions an average transmissibility of $\sim 5 \times 10^{-15} \text{ m}^3$ and an effective permeability of $\sim 1 \times 10^{-17} \text{ m}^2$ have been deduced for the open hole section (length: 371 m). Further analysis using a specialized plot “ ΔP vs. $\Delta t^{(1/4)}$ ” shows a clear indication of bilinear flow suggesting that the flow regime is dominated by a few fractures (Bourdet, 2002).

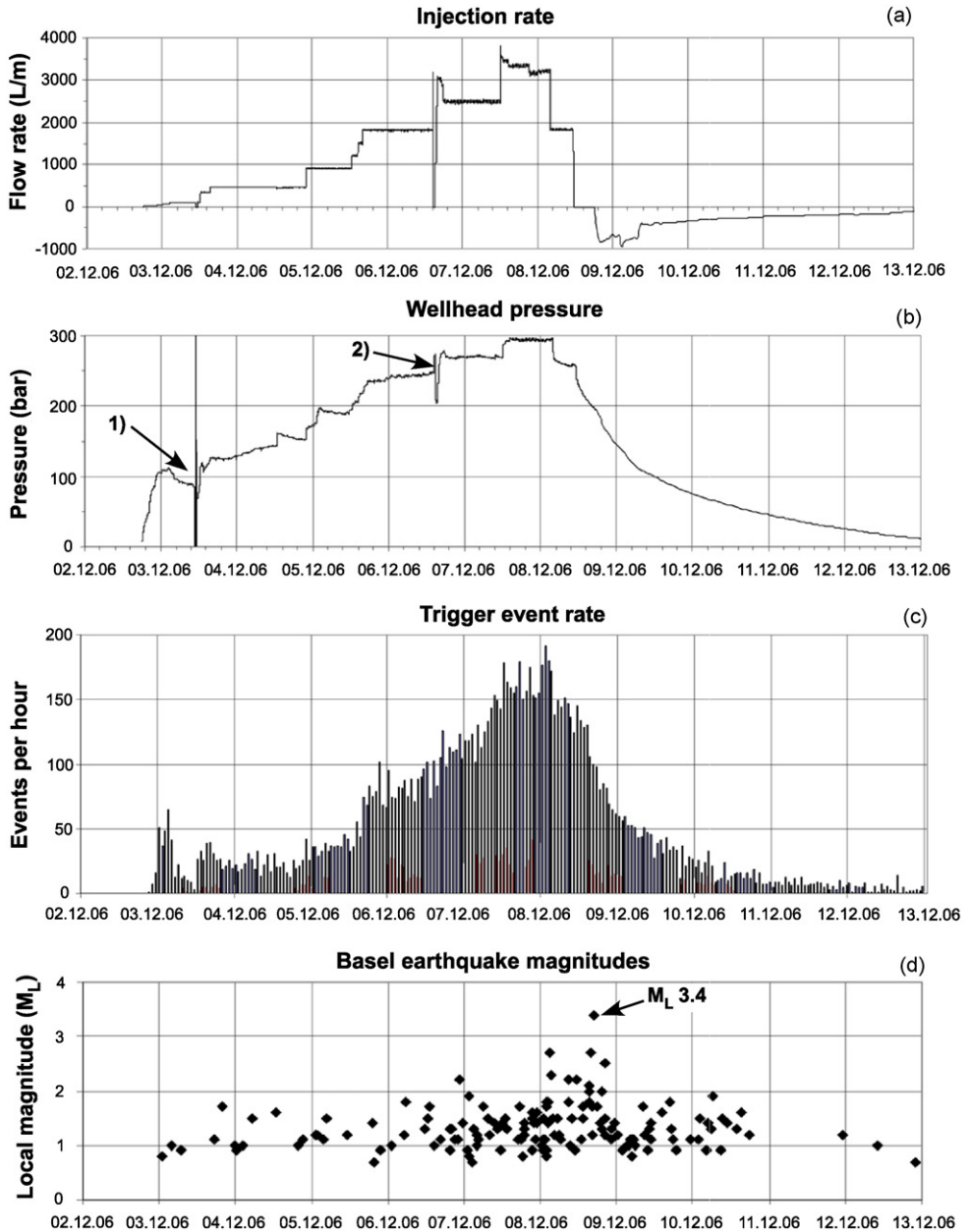


Fig. 5. Data on the hydraulic stimulation of well Basel 1. History of (a) injection rates, (b) wellhead pressures, (c) trigger event rates and (d) Basel earthquake magnitudes as determined by Swiss Seismological Survey (SED). In panel (b), Transient 1 is due to a change in injection pump, and Transient 2 to the repair of a leaking wireline blowout preventer.

2.5. Hydraulic stimulation

Starting on 2 December 2006 the Basel 1 well was stimulated with a massive injection of 11,570 m³ of river water that was taken from a nearby harbour basin in the Rhine River.

Over the first 16 h the flow rate was increased in steps from 0 to 100 L/min resulting in a wellhead pressure of 110 bar (Fig. 5). In the following days the flow rate was increased gradually up to a maximum of 3300 L/min resulting in a wellhead pressure of 296 bar. The seismic activity in the reservoir increased with rising pressure and flow rate, and reached magnitudes that required a reduction in flow rate and the eventual well shut-in as laid down in the approved microseismic response procedure (see Section 3.2). Due to the high seismic activity, the injection rate was reduced in the early morning of 8 December 2006, after 6 days of continuous injection. Five hours later it was decided to shut-in the well as the seismic activity remained at an unacceptably high level, although without excessive magnitudes. This measure was not sufficient to produce a rapid drop in the frequency of events $>M_L$ 1, so it was decided to bleed-off the well as a precaution; a M_L 3.4 event occurred just before starting the bleed-off. In response to bleeding the well the pressure dropped to hydrostatic within 4 days. The well has since remained open, producing a cumulative backflow of about 3400 m³ over a 14-month period.

In the entire stimulation process the wellhead pressure build-up in relation to flow rate was most prominent below 80 bar wellhead pressure, indicating poor injectivity. Above 80 bar and with higher flow rates, the injectivity improved indicating a coupled hydro-mechanical response of the rock mass. The highly irregular wellhead pressure curve (Fig. 5) is thought to reflect shear slipping on nearby optimally oriented pre-existing fractures, resulting in sudden increases in injectivity close to the wellbore. Above 235 bar, pressure variations become less erratic. This might be regarded as indicating that shear-induced permeability enhancement was occurring at ever increasing distances from the wellbore, and/or an increasingly elastic response of fractures in the reservoir due to changes in effective normal stress (Rutqvist and Stephansson, 2003). As long as the overpressure is kept high, both shear slipping and elastic response of the fractures are assumed to contribute to an enhancement of the fracture permeability and to control the development of the Basel 1 reservoir.

No conclusive assessment of the efficiency of the stimulation in Basel 1 can be given because no hydraulic post-stimulation tests have been conducted since the suspension of the operations. From the preliminary data set, however, the extent of fracture transmissibility enhancement was estimated by investigating pressure and backflow changes due to manipulations of the choke manifold during the bleed-off phase, in a manner similar to that of a production test with variable flow rates. The change in fracture transmissibility can be calculated using the equation (Jung and Ortiz, 2007):

$$\frac{T_{F,i}}{T_{F,0}} = \left(\frac{\Delta Q_i}{\Delta Q_0} \right) \left(\frac{\Delta p_0}{\Delta p_i} \right) \quad (3)$$

where $T_{F,i}$ is the fracture transmissibility for step i , $T_{F,0}$ is the initial fracture transmissibility, ΔQ_0 is the difference between the actual flow rate and the flow rate of the initial low-rate injection test, and Δp_0 is the difference between the actual pressure and the pressure of initial low-rate injection test.

Applying Eq. (3) to our data set led to the conclusion that the fracture transmissibility had increased by a factor of approximately 400 and that this enhancement proved irreversible throughout the bleed-off phase.

3. Microseismic characterization of the Basel 1 reservoir

3.1. Microseismic monitoring network

The microseismic monitoring network array was carefully designed using numeric modelling techniques. The objective was to achieve an optimal balance between network sensitivity, network resolution, operational reliability and financial constraints. Network sensitivity modelling provided an estimate of the seismometer depths required to achieve a reasonable signal-to-noise (S/N) ratio at all the potential observation stations for a simulated model event with a moment magnitude of 0.8 at a reservoir depth of 5 km. To model realistic S/N ratios the simulation of the wavefield propagation included anelastic attenuation, wavefield scattering and geometrical spreading (Hölker and Graf, 2005). The depth-dependent attenuation functions used in the modelling were derived from a Vertical Seismic Profile (VSP) survey in the geothermal exploration well OTER2 (Hölker et al., 2005). Furthermore, in deciding where to set up the microseismic network stations, the ambient background noise level at the surface for potential observation sites was recorded and evaluated for characteristic day and night times (Hölker, 2005).

The network station geometry was further optimized with a network resolution modelling technique (Dyer et al., 2008). This simulation was based on an estimate of the random error for the travel-time determination of P- and S-wave arrivals, which was set to be ± 8 ms for P- and S-waves (Dyer et al., 2008). The station geometry was refined such that the modelled relative network resolution for absolute located events was about 100 m.

The implemented monitoring network comprises an array of six borehole stations ranging from 320 m to 2745 m depth (Fig. 1). Each seismic monitoring station is equipped with a downhole three-component geophone designed to withstand temperatures of up to 125 °C and pressures of up to 345 bar in long-term operation. Apart from the deep monitoring station at 2745 m in OTER2, the geophone sensors are combined with three-component Micro-ElectroMechanical Sensors (3C MEMS) in order to cover a larger magnitude range without instrument saturation effects. The continuous data stream is digitized at the individual observation sites and transferred via a Virtual Private Network link to a central server unit.

During the active hydraulic stimulation a two-step data processing procedure was applied. First, an automatic real-time processing routine was used, including event detection, determination of P- and S-wave onset times, absolute hypocenter location and moment magnitude calculation. Second, a near real-time visual control of the automatically determined travel time picks was conducted and – where required – the events subsequently relocated. Applying tight event location criteria (P- and S-wave times were required for the same four monitoring stations together with a low travel-time residual) consistent absolute event locations were achieved, with an absolute accuracy of about 100 m. Thus the spatio-temporal reservoir development could be reliably imaged in near real-time.

3.2. Seismic response procedure

Since the planned EGS system is located in an urban area, real-time monitoring of seismic events was critical. State-of-the-art techniques, designed for monitoring increased levels of induced seismicity, were investigated. The historical level of natural seismic activity within the Basel region was also evaluated. The current local stress field was investigated by analyzing focal mechanisms of natural events within the area of interest (Evans and Roth, 1998). This study as

well as other research work (e.g. Plenefisch and Bonjer, 1997, Kastrup et al., 2004) indicates that the DHM Project is located in a strike-slip dominated stress regime (c.f. Fig. 4) with a minor normal faulting component.

Prior to any hydraulic tests in well Basel 1, a thorough study was carried out to define an appropriate response procedure at predefined levels of induced seismic activity during the stimulation operation. This study was required as part of the process of obtaining permission to proceed from the regional government of Kanton Basel-Stadt.

The basic concept of the seismic response procedure has been adapted from the “Traffic Light System” proposed by Bommer et al. (2006). Correspondingly, the DHM seismic response procedure is based on three independent parameters:

1. Public response
2. Local magnitude (M_L)
3. Peak ground velocity (PGV)

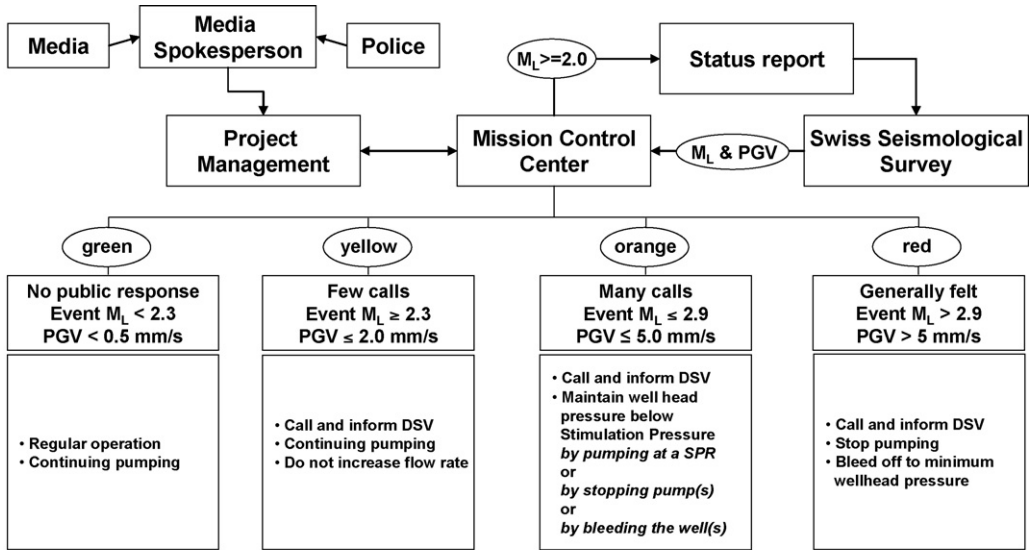
In order to predefine appropriate thresholds for M_L and PGV, the potential ground motion at the Basel site was simulated (Rutishauser, 2006) using seismic event data from the Soultz-sous-Forêts project (located 150 km north of Basel, still in the Upper Rhine Graben) corrected for local near-surface amplification effects in and around Basel City (Giardini et al., 2004). The proposed seismic response procedure was discussed with international experts and approved by the local authorities. A summary of the agreed thresholds and the appropriate responses is given in Fig. 6.

During the stimulation operations the M_L and PGV values were determined by the Swiss Seismological Service (SED) as an independent institution. Near real-time alert information was provided by email and mobile phone, and was visualized on a web-based CISN display (California Integrated Seismic Network) in the processing and control center.

3.3. Reservoir mapping and event magnitudes

Seismic activity was first detected about 3.75 h after the start of the stimulation operation (Fig. 5). The volumetric reservoir development began near the casing shoe of the well. Hypocenter locations of the very early events were focused around a hydraulic infiltration zone at 4422 m bOD (below Ordnance Datum, which is at 250 m depth) verified by repeated pressure–temperature–spinner flowmeter (PTS) log runs during the injection phase. With the continuation of the stimulation process, the event hypocenter locations migrated preferentially along a NNW-SSE-trending structure (Fig. 7). The event rate reached its peak value of about 200 events per hour at the maximum injection rate of ~ 3300 L/min (Fig. 5).

Absolute event hypocenter locations were determined by an exhaustive grid search algorithm. An initial coarse location was found using a 25-m cubic grid; a 2-m cubic grid was used to refine the location. At each grid point the P and S times were found by ray tracing through the layer velocity model. These model times were compared to the observed times in a least squares manner to find the grid point with the minimum combined P and S time misfit. For every location, P and S times from stations Haltingen (HALTI), Schützenmatte (MATTE), Riehen 2 (RIEH 2) and Otterbach 2 (OTER 2) (see Fig. 1 for station locations) were required (the P times from the deep geophone in Basel 1 were also used when this receiver was deployed). For consistency in locations, any other times were excluded. The hypocenter locations have a maximum root-mean-square (rms) misfit of 10 ms. Events with larger misfits were not located (Dyer et al., 2008).



Explanation:

M_L – Local magnitude (provided by the Swiss Seismological Survey; SED)

PGV – Peak ground velocity (provided by the Swiss Seismological Survey; SED)

DSV – Drilling supervisor

Stimulation Pressure – Wellhead pressure where the first induced event occurs

SPR (Slow Pump Rate) and Stimulation Pressure to be defined in 48 hour look ahead every day

Fig. 6. Seismic response procedure during the stimulation phase of the Deep Heat Mining Operation 2006. Measures to be taken at predefined threshold levels for local magnitudes and peak ground velocities are specified and the communication flow within the system is indicated.

Within the time frame of active stimulation (2–8 December 2006) some 11,200 events were detected, of which more than 2400 could be reliably located in near real-time (Fig. 7). After the well bleed-off the seismic event rate declined only gradually, resulting in an additional (post-injection) increase in the volume of the seismic cloud of approximately 75%. Up to the end of November 2007, about 3700 additional events were recorded of which more than 1100 could be located (Fig. 7).

The image of the seismically active volume displays a steeply dipping lens-shaped structure trending $N155 \pm 5^\circ E$ and a single offsetting branch with an azimuth of $N100 \pm 10^\circ E$ (Fig. 7). The narrow shape of the mapped post-stimulation event structure in the SSE reservoir section confirms that the absolute location uncertainty in some reservoir sections seems to be much lower than the predicted location error of 100 m. The reservoir extends about 1 km along the dominant reservoir azimuth and about 1 km in depth. By summing up all the 25-m sided cubic cells that enclose at least one microseismic event, we estimated a seismically active reservoir volume of approximately 35 million m^3 .

Moment magnitudes, calculated in the frequency domain, range from $M_w \approx 0$ to $M_w \approx 3$. The observed network sensitivity is significantly better than the modelled threshold magnitude of M_w 0.8. Based on a best-fit correlation, all moment magnitudes have been transferred into the local magnitude (M_L) scale, allowing the classification of the whole range of M_w for located events

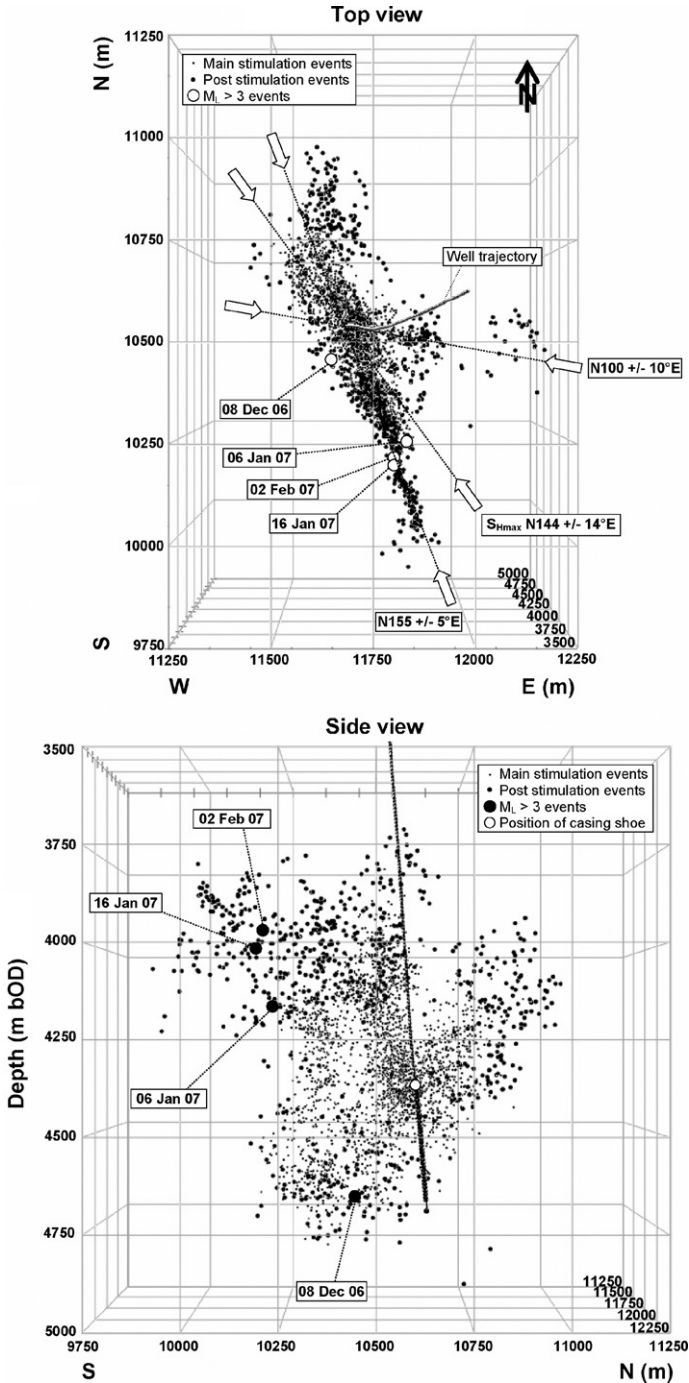


Fig. 7. Absolute locations of seismic events from the active injection phase (2–8 December 2006) and the post-stimulation phase (8 December 2006 up to the end of November 2007). The hypocentral locations of the M_L 3.1–3.4 events are highlighted and the dominant reservoir strike directions are displayed together with the azimuth of the principal horizontal stress component S_{Hmax} . Depths are given in meters below Ordnance Datum (bOD), which is at 250 m depth.

within the regional magnitude scale of the SED (Bethmann et al., 2007). The resulting local magnitudes span a range of $-1 \leq M_L \leq 3.4$.

3.4. Fault plane solutions

The fault plane solutions for a number of selected events have been analysed to address two questions:

1. Do the active rupture surfaces correspond with the orientation of tectonic structures and are they consistent with the current stress field around Basel?
2. Do the interpreted nodal planes match the spatial orientation of event clusters that are formed by events of mutually coherent waveforms, so called multiplets?

The results of these investigations provide a valuable insight into the geomechanical rock behaviour at the Basel site and are regarded as key data for future seismic risk studies as well.

The focal mechanisms have been studied based on P-wave first-motion polarity observations. To date, focal mechanisms for 27 events have been analysed, covering the magnitude range $1.7 \leq M_L \leq 3.4$ (Deichmann et al., 2007a). The fault plane solutions were constrained by integrating the observations of the maximum available number of seismic station recordings from the SED and the Erdbendienst des Landesamtes für Geologie, Rohstoffe und Bergbau Baden-Württemberg in Freiburg (LED) together with the observations of the microseismic monitoring network. In addition, these institutions operated a large number of temporary stations during the stimulation phase. For the largest events, up to 80 first-motion polarity observations could be used to determine the fault plane solutions (Fig. 8).

Of the 27 events analysed so far, 24 fault plane solutions can be interpreted as either left-lateral strike-slip on predominantly NS-trending fault planes or alternatively right-lateral strike-slip on predominantly EW striking fault planes (Fig. 9). A small set of two fault plane solutions exhibits a major normal faulting behaviour with a minor strike-slip component on roughly NW-SE-trending structures. One event has been interpreted as an oblique focal mechanism of combined normal faulting and strike-slip. These observations provide independent evidence that the reservoir is situated in a strike-slip dominated stress regime, which is in line with the above reported stress analysis results (Plenefisch and Bonjer, 1997; Evans and Roth, 1998; Deichmann et al., 2000; Kastrup et al., 2004, and Fig. 4).

The optimal shear angle is a function of friction coefficient μ , both for failure of intact rock and slip of pre-existing faults. As generally agreed, μ almost always ranges between 0.6 and 1.0. Thus, the optimal angle between S_{Hmax} and fault strike should lie in between about 22° and 30° , both for intact and pre-fractured rock. With respect to the direction of S_{Hmax} of $N144 \pm 14^\circ E$, the optimal angles for strike-slip in the DHM reservoir are around $N166-174 \pm 14^\circ E$ and $N122-114 \pm 14^\circ E$. The nodal planes of the strike-slip fault plane solutions are close to vertical, trending approximately NS and EW (Figs. 8 and 9). It seems as if slippage has been induced on discontinuities of somewhat non-optimal orientations, which may indicate that the sheared structures are weaker than the surrounding rock.

Normal faults are expected to form conjugate pairs that dip around 60° and strike parallel to S_{Hmax} (Zoback, 2007). This criterion is fulfilled for the two interpreted normal fault focal mechanisms.

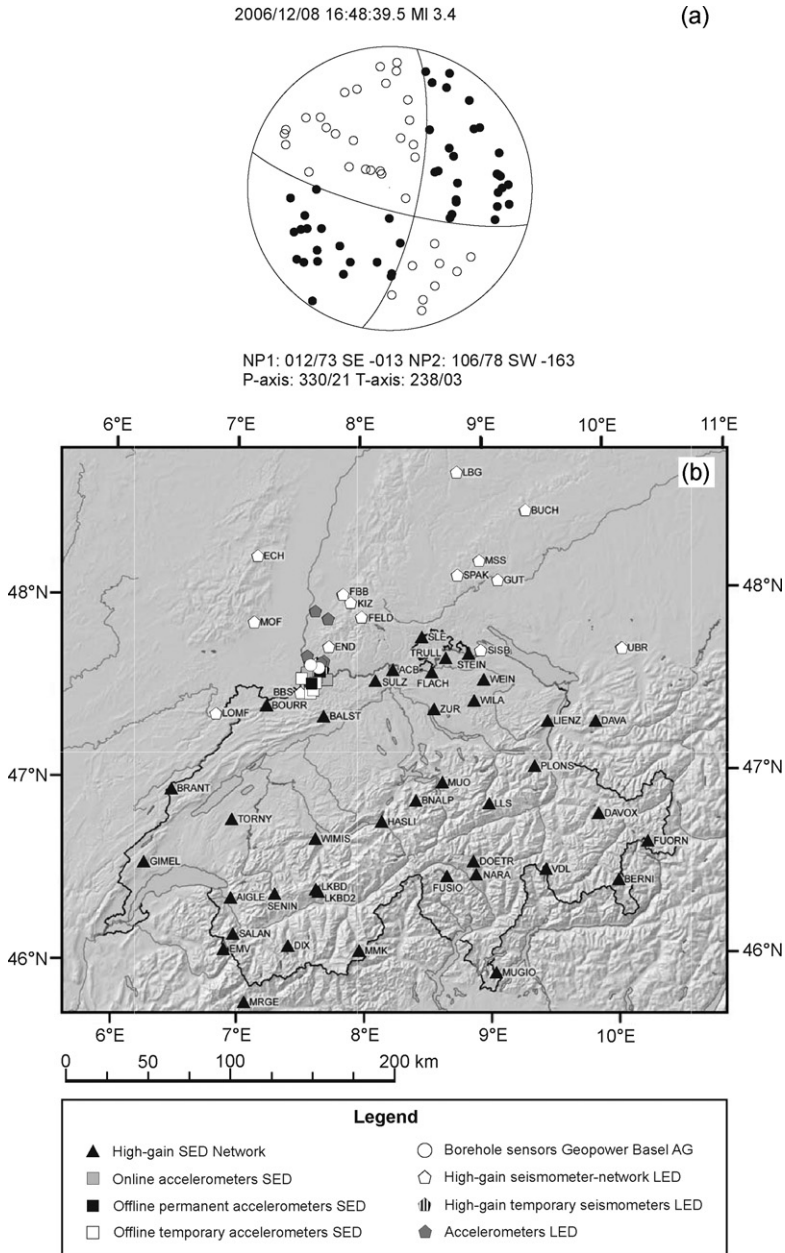


Fig. 8. (a) Fault plane solution for the largest event (M_L 3.4). P-wave first-motion polarity observations are shown as equal-area projections to the lower hemisphere (modified after Baer et al., 2007). Black circles denote compressive first-motion (up) and open circles represent dilatational first-motion (down). The text at the top of the panel specifies date, time and local magnitude of this event. The text below the panel denotes strike, dip and rake of the two nodal planes (NP1, NP2) and the azimuth and plunge of compressional (P) and extensional (T) axes. (b) Map of all potential seismic stations from which recordings were used to infer fault plane solutions (modified after Deichmann and Bachmann, 2007b). The map includes the regional networks of the Swiss Seismological Service (SED) and the Erdbendienst des Landesamtes für Geologie, Rohstoffe und Bergbau Baden-Württemberg in Freiburg (LED) and the borehole station array of Geopower Basel AG.

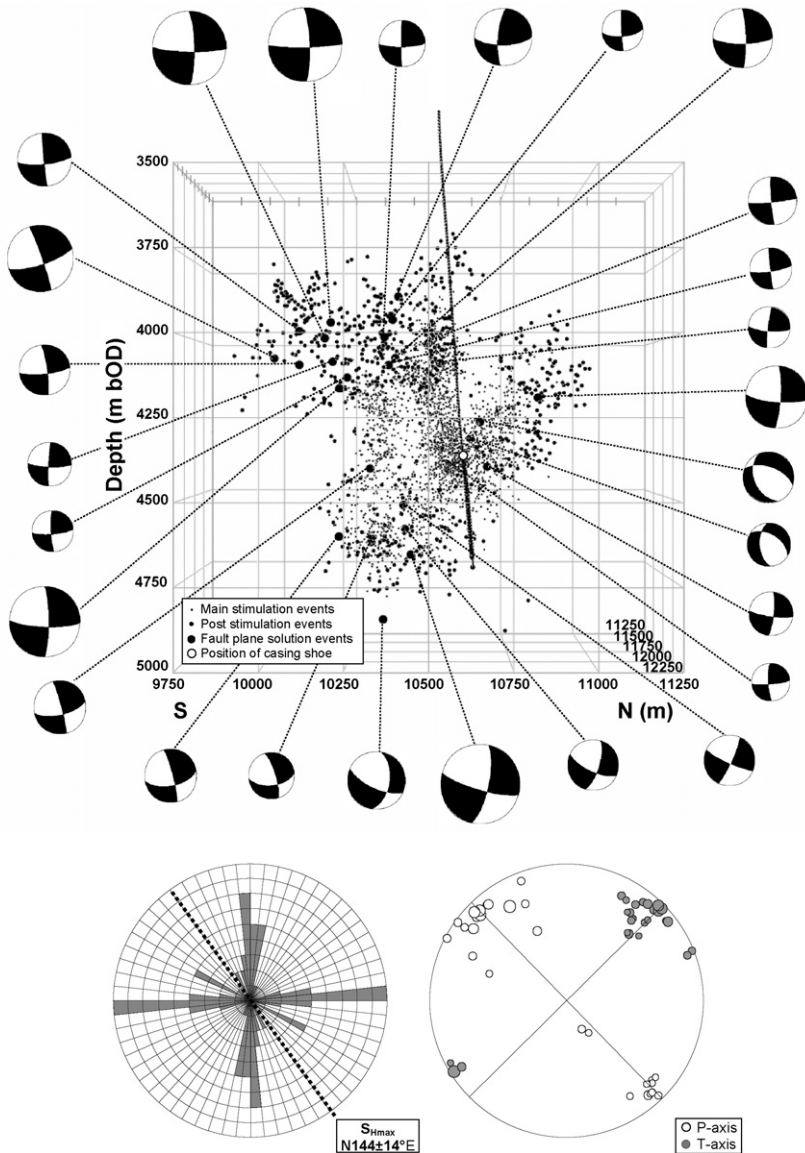


Fig. 9. Upper panel. Fault plane solutions for event magnitudes in the range $1.7 \leq M_L \leq 3.4$. The fault plane solution spheres are scaled in proportion to the event magnitudes. Depth values are given in meters below Ordnance Datum (bOD), which is at 250 m depth. Lower panel. Rose diagram showing the azimuthal distribution of the nodal planes and orientation of S_{Hmax} (left) and the distribution of P-(compressional) and T-(dilatational) axes (right) (modified after Deichmann et al., 2007a).

Clusters of similar events, referred to as multiplets (Kumano et al., 2007), may be found by waveform coherency analysis. Such clusters are expected for events that have similar travel paths and focal mechanisms. Thus, multiplet clusters are considered to represent discrete structures on which repeated shear processes have occurred. Under this assumption the orientation of the

multiplet cluster indicates the orientation of the active nodal plane and may be compared with the fault plane solutions of events within the cluster.

So far, four multiplet clusters that include fault plane events have been identified. Three of these clusters trend approximately NS and one EW (Fig. 10) in agreement with the available fault plane solutions within each of the clusters. For these clusters, NS- and EW-trending nodal plane azimuths are also supported by the observed event waveform characteristics. The waveforms recorded at the station HALTI, which is located north of the reservoir show small P-wave and comparatively large S-wave amplitudes. In comparison, the signals recorded at the station MATTE, which is located southwest of the reservoir, have larger P-wave amplitudes and relatively small S-wave amplitudes (Fig. 10). These amplitude ratios are consistent with a traditional double-couple radiation pattern for NS- and EW-trending nodal planes. In conclusion, the mapped cluster orientations, waveform attributes and fault plane solutions are consistent with shearing on near NS- and EW-aligned structures.

More extensive multiplet analysis is in progress in order to constrain and test these preliminary results further.

3.5. Events with increased magnitudes

The Basel 1 well-stimulation operation was accompanied by some seismic events that were clearly perceived by the public; the largest (M_L 3.4) occurred on 8 December 2006. In line with the seismic response procedure the operation was suspended. Three aftershocks with $M_L > 3$ occurred on 6 and 16 January 2007 and on 2 February 2007; respectively 29, 39 and 56 days after shut-in and subsequent well bleed-off.

For the future of EGS we regard it as critical to understand the mechanisms of hydraulically induced shearing processes and their related seismic effects, not only in the subsurface but also at the surface, as they impact society and may create a potential seismic hazard. The extensive seismic and hydraulic data set that has been acquired in Basel provides a unique opportunity for in-depth research into the processes involved.

3.6. Potential mechanisms

Based on observed characteristic waveform signatures, the largest events may have formed by a cascade-like rupture process. A clear stair-step build-up can be seen on the P-wave first-motion amplitude of the M_L 3.4 event recorded at seismic observation station OTER2 (Fig. 11). This might indicate the superposition of radiated seismic energy resulting from a number of discrete successive events a few milliseconds apart. Station OTER2 is located closest to the event hypocenter and is the only monitoring station where the incipient amplitudes of the individual event signals are resolved. The direct P-waves recorded at the more distant stations are interpreted as the envelope amplitude of the stacked-up discrete event signals.

A similar stacking effect – but with larger time shifts between individual events – is characteristic of the M_L 3.1–3.2 aftershock events (Fig. 11b–d). For these events at least three discrete P-wave arrivals are discernible on the traces of all stations. For comparison, Fig. 11e shows the traces from the largest event with no apparent multiple arrivals (M_L 2.2).

The driving mechanism for these cascade events can be explained in two ways. First, a cascade-like rupture process may have taken place by near-synchronous shearing of several critically pre-stressed fracture patches in very close proximity along a single rupture surface. Second, it

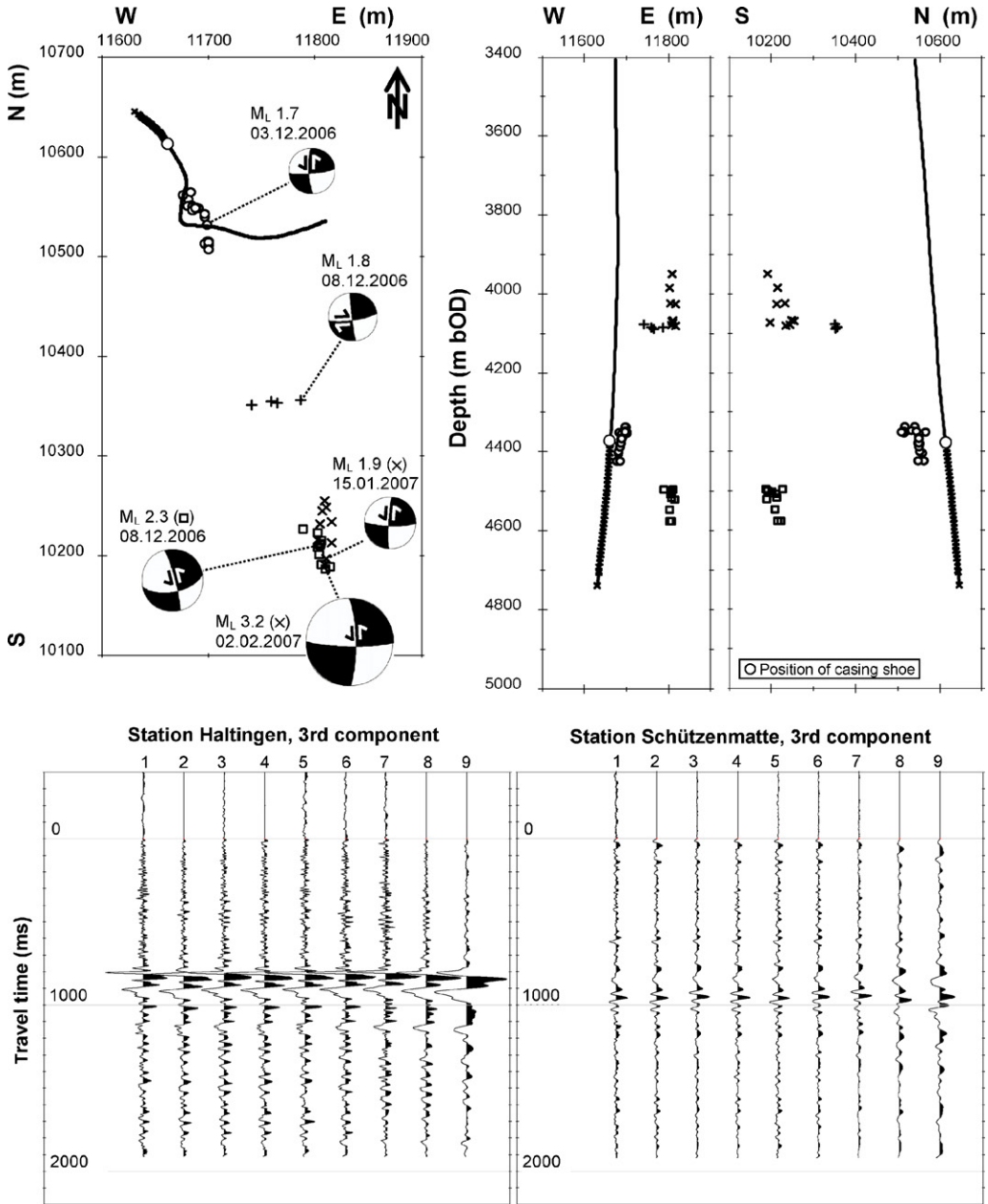


Fig. 10. Upper panels. Horizontal (left) and two vertical projections (middle and right) of multiplet clusters that include fault plane solution events. The corresponding fault plane solutions are shown together with the interpreted active nodal plane and the sense of displacement. Depth values are given in meters below Ordnance Datum (bOD), which is at 250 m depth. Bottom panels. Waveforms of the multiplet cluster marked by exes (x) in the upper panels recorded at two distinct monitoring stations. The station Haltingen (HALTI; Fig. 1) lies approximately in line with a NS-trending nodal plane through the stimulated reservoir, whereas the station Schützenmatte (MATTE; Fig. 1) is located SSW of the reservoir volume. The P-wave arrivals have been aligned at time zero and the S-waves arrive at 800–900 ms. The observed P- to S-wave amplitude ratios are consistent with the radiation pattern of NS- and EW-trending nodal planes.

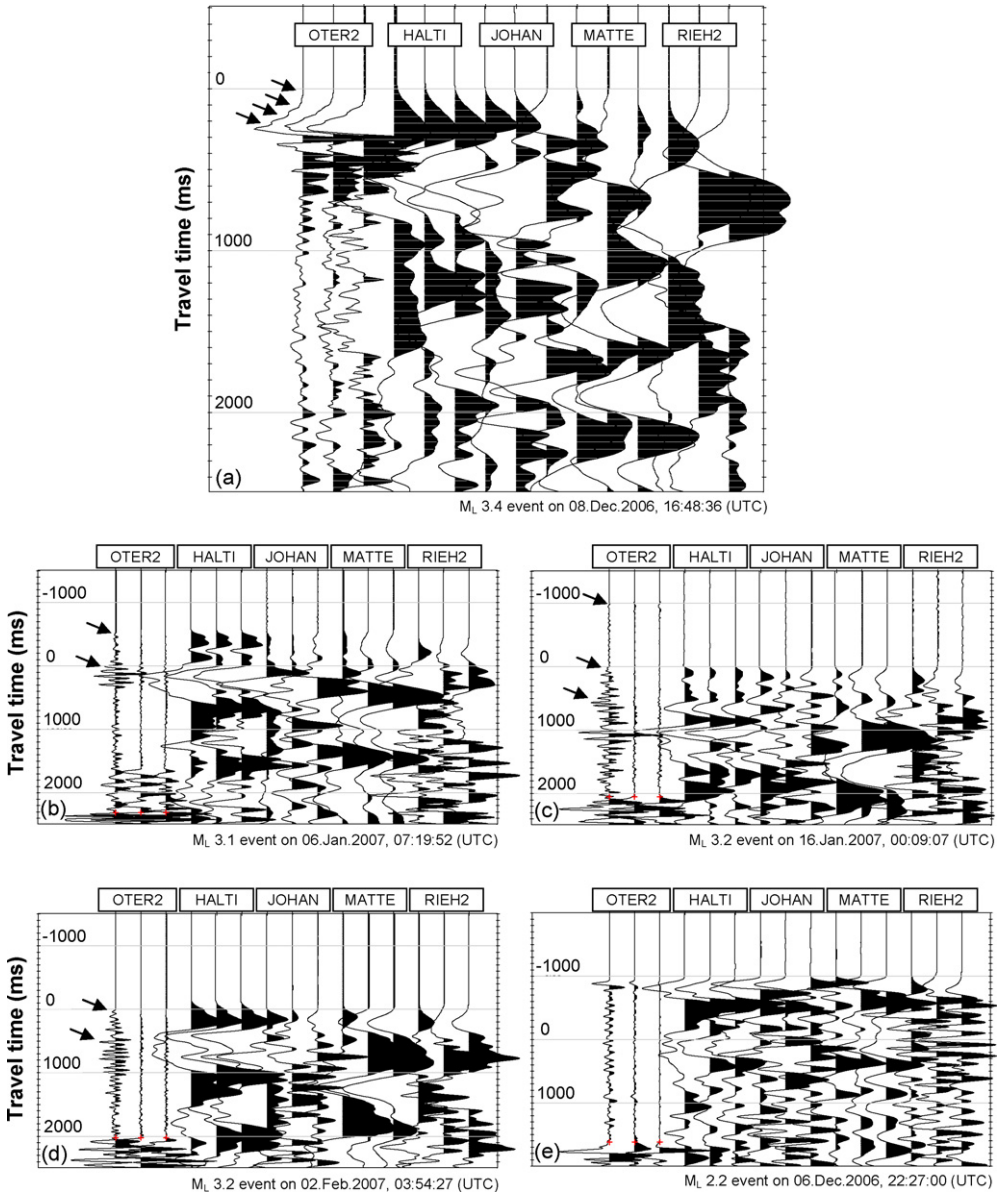


Fig. 11. Raw, unfiltered traces (a) for the M_L 3.4 event, (b–d) for the M_L 3.1–3.2 aftershock events and (e) for the largest observed event with no apparent multiple arrivals (traces plotted with trace-to-trace scaling; multiple arrivals are indicated by arrows). The traces of the different stations were aligned at the P-wave picks. (a) A number of successive events a few milliseconds apart appear to have stacked together producing stair steps in the P-wave amplitude recorded at station OTER2. (b) There is a smaller arrival at -60 ms on all sensors followed by the picked arrival at 0 ms. (c) The recordings at OTER2 show a very small arrival at -100 ms, followed by the picked arrival at 0 ms and at least one further arrival at around 50 ms that is apparent on all sensors. (d) The picked arrival at 0 ms is followed by another arrival at around 50 ms. The locations of the seismic stations are shown in Fig. 1.

might be that the stacked events were due to near synchronous shearing of individual structures that are not lying along the same surface but are subparallel.

3.7. Source radius

The sizes of the event rupture surfaces, the source radii, have been calculated from the corner frequency of the signal displacement spectrum (Madariaga, 1976). For the M_L 3.4 event a source radius of 101 m and a rupture area of 32,000 m² were estimated. For a natural event of the same magnitude and a typical stress drop in the range 1–100 bar, a source radius of between 145 m and 670 m is expected, assuming circular rupture (Eshelby, 1957). This indicates that in our case a stress drop of approximately 300 bar is not unlikely, which is consistent with the estimated large differential stress at the event depth of 4966 m (cf. Fig. 4).

The idea that elevated differential stress may produce a higher probability for the occurrence of increased event magnitudes is supported by results discussed in Schorlemmer et al. (2005). Based on a statistical evaluation of high-quality natural earthquake data sets, these authors could show a dependency of the earthquake size distribution (Gutenberg-Richter b -value) on focal mechanism, a relation that follows the priority: $b_{\text{thrust faulting}} < b_{\text{strike-slip faulting}} < b_{\text{normal faulting}}$.

Schorlemmer et al. (2005) infer an inverse relationship between the magnitude of the differential stress prevailing at the subsurface and the b -value of an event sequence at a given location site. In that sense this value is considered to act as a “stress meter”, e.g. indicating stress accumulation at locked fault patches. These authors also point out that the influence of differential stress upon the b -value is supported by a number of referenced empirical observations, in the laboratory and from mines, which could be explained by a physical model and model simulations as well.

4. Geomechanical reservoir model

4.1. Rock mass stability analysis

Rock mass stability and the potential for failure or slip is best shown on Mohr diagrams. The Mohr circles are based on the generalized effective stress law,

$$S_{\text{eff}} = S_{\text{tot}} - \alpha P_P \quad (4)$$

where S_{eff} is the effective stress, S_{tot} is total stress, α is the Biot constant and P_P is the pore pressure.

In weak rocks or along pre-existing fractures α tends towards 1, whereas in hard rock with low porosity α is significantly less than 1 (Fjaer et al., 1992). A coefficient α of 0.2 has been determined from laboratory tests on an intact drill core sample from the reservoir section of Basel 1 (Braun, 2007). Additionally, the intact rock strength was determined in the laboratory by a multistage test on the same core sample (Fig. 12a).

The rock mass stability analysis is performed with total stress estimates for $S_{H_{\text{max}}}$ equal to 160 MPa (lower bound estimate as discussed in Section 2.3) and $S_{H_{\text{min}}}$ equal to 84 MPa (derived by RACOS[®]). For hard rock a coefficient α of 0.2 is assumed. Pore pressure increase results in a slight shift of the Mohr circle to the left. The shear failure criterion is not exceeded and thus no shearing is expected to take place in the intact rock mass (Fig. 12a).

Nonetheless, the microseismic monitoring demonstrated that shearing did take place. This could only have occurred at rocks with reduced frictional strength and/or a coefficient α closer

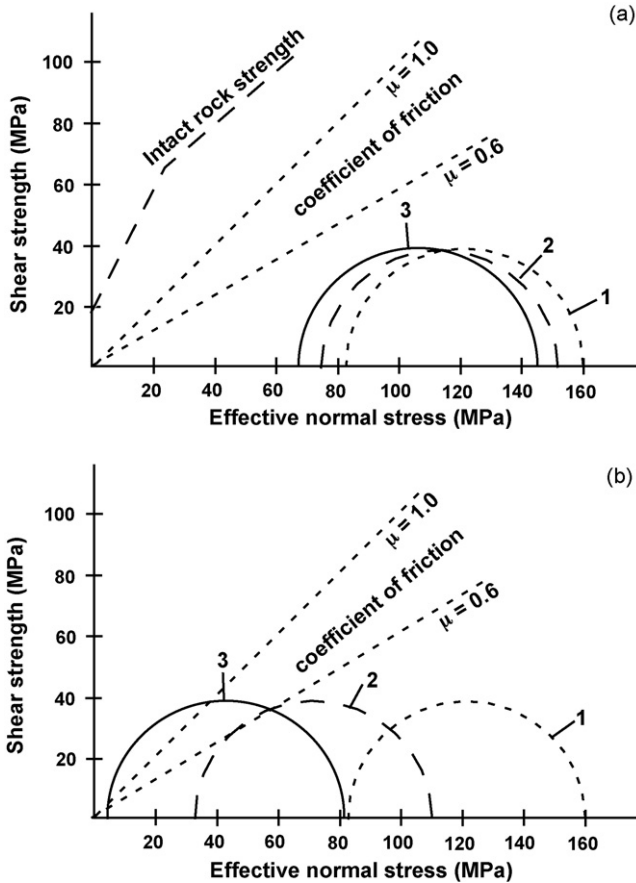


Fig. 12. Mohr diagrams illustrating the effect of increasing pore pressure depending on the coefficient α (see Section 4). (a) Mohr circles for hard rock with low porosity ($\alpha = 0.2$) at total stress conditions (Circle 1); effective stresses at hydrostatic conditions during hydraulic stimulation (Circle 2); effective stresses at maximum overpressure conditions during hydraulic stimulation (Circle 3). (b) Mohr circles for weak rock ($\alpha = 1$) (e.g. cataclastic fracture zone) at total stress conditions (Circle 1); effective stresses at hydrostatic conditions (Circle 2); effective stresses at maximum overpressure conditions during hydraulic stimulation (Circle 3).

to 1; if it is equal to 1 it significantly increases the effect of pore pressure (Fig. 12b). From the acoustic borehole imager we know that two cataclastic fracture zones are present within the open hole section of well Basel 1. Such weak zones are expected to have both a reduced frictional strength and a coefficient α closer to 1. Therefore, we assume that shearing took place within such cataclastic fracture zones.

4.2. Preliminary working model

Based on the preceding observations and analysis the following working model is proposed. The dominant part of the stimulated Basel 1 reservoir volume has developed along a pre-existing cataclastic fracture zone striking NNW-SSE. This inference is supported by the fact that the earliest microseismic events occurred at 4672 m depth, very close to the upper cataclastic fracture

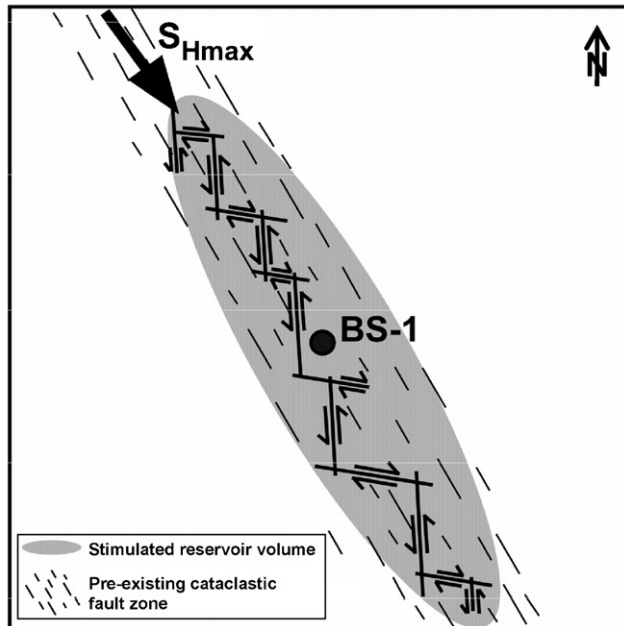
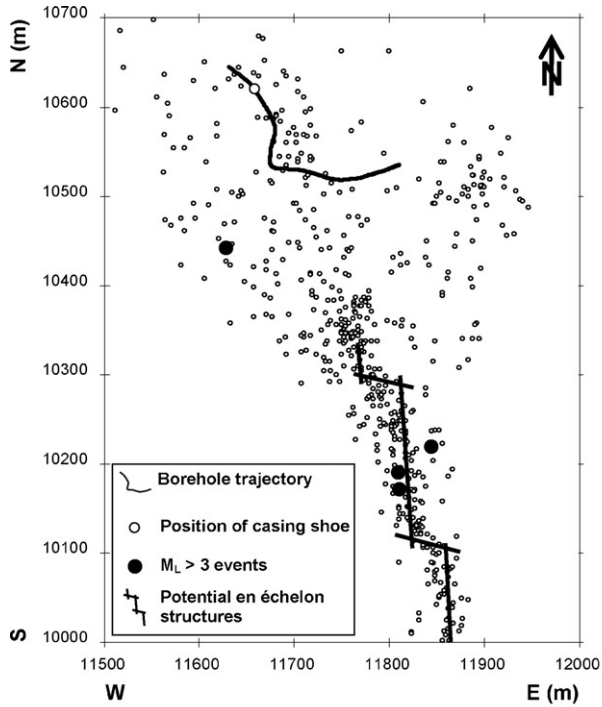


Fig. 13. Top panel. Horizontal projection of the post-stimulation event locations. Possible alignments in the seismicity trending NS that are interlinked with more EW-trending structures are overlain. Bottom panel. Schematic model of reservoir development in an assumed pre-existing cataclastic fracture zone. Fault plane solutions of medium-to-large events indicate that frictional sliding has been induced on roughly NS- and EW-trending structures that are ordered in an en échelon like arrangement. BS-1: well Basel 1.

zone identified by the acoustic borehole imager. The maximum horizontal principal stress (S_{Hmax}) appears to be approximately in line with this NNW-SSE direction, so that no shear processes should take place along the fault axis. Most of the analysed fault plane solution events were generated by shear processes on structures arranged “en échelon” with alternating NS and EW directions along the presumed cataclastic fracture zone (Fig. 13). The NS oriented fault plane solutions show left lateral strike-slip and the EW-trending structures right lateral strike-slip. There is further evidence for this model in the southern section of the reservoir, which developed during the post-stimulation phase (Fig. 13) where NS-trending segments interlinked by EW-trending segments may be interpreted.

5. Conclusions and outlook

The Basel 1 reservoir is composed of a granitoid rock, which is intersected by steeply dipping discontinuities with a dominant NW-SE to NNW-SSE strike direction. In the open hole section two cataclastic fracture zones were encountered that are both affected by argillitic alteration. The reservoir can be characterized by a low-permeability rock matrix plus a few water-conducting features.

The orientation of S_{Hmax} in Basel 1 is NNW-SSE and nearly coincides with the azimuth of the dominant fracture set. The stress regime is predominantly strike-slip with relatively high deviatoric stresses following the hierarchy $S_{Hmax} > S_V > S_{hmin}$. The vertical stress is well defined from the overburden density. The magnitudes for the two horizontal stresses S_{hmin} and S_{Hmax} are still uncertain but they have been constrained using different techniques.

The shape of the seismically active zone can be described as a near-vertical lenticular feature with an ESE offsetting branch. The seismically active volume is of the order of 35 million m³, which was created by the injection of 11,570 m³ of water over a period of 6 days.

We infer that the main part of the reservoir has evolved along a pre-existing shear zone trending NNW-SSE. As this nearly coincides with the direction of the maximum horizontal principal stress (S_{Hmax}) virtually no shear stress is acting on the main shear zone itself. Hence, no frictional sliding is happening along this feature, as indicated by the near absence of earthquake nodal planes striking in a NNW-SSE direction. The probable explanation is that under increased pore pressure conditions the rock mass stability in the cataclastic fracture zone is reduced. Within this narrow zone induced shearing appears to have taken place in NS and EW directions in an en-échelon pattern of strike-slip faults. This hypothesis is supported by earthquake nodal plane orientations and preliminary multiplet cluster orientations. The overall reservoir development is confined to a relatively narrow plane.

Rupture processes for events with $M_L > 2.2$ appear to have occurred in cascades either on single continuous structures or nearly synchronously on several closely adjacent structures, as suggested by the apparent stacking of direct P-wave arrivals.

The integration of probabilistic parameters in designing a seismic hazard response for this and other EGS sites seems to be of considerable value. Wiemer et al. (2007) analysed retrospectively the statistical behaviour of the induced seismic event sequence. The results suggest that a real-time earthquake hazard assessment appears to be a promising option that needs to be proved in future EGS projects. It may provide an independent means of evaluating critical levels of induced seismic activity. However, this requires detailed previous knowledge of statistical parameters that are critical for estimating earthquake probabilities in real-time. Therefore, a preliminary statistical parameter evaluation might be done based on the event sequence induced during a small-scale stimulation operation in the run-up to the main stimulation activity. Furthermore, a well-defined

calibration of moment magnitudes from the monitoring system with regionally defined local magnitudes is essential.

The development of an alternative stimulation concept is a key to mitigating seismic risk from hydraulic stimulations. The significant increase in reservoir volume in the post-stimulation phase led to the idea of initiating shear processes by injecting a limited fluid volume over a short time period, venting the reservoir and subsequently monitoring the resulting events. This “nudge and let it grow” procedure could be applied repeatedly; a strategy that may be somewhat time-consuming but might help to minimise perceptible induced events in EGS.

The original concept of generating a network of densely distributed fractures that are efficiently hydraulically interlinked over a large rock volume with one massive hydraulic injection has to be reviewed. The results show that the predominant reservoir development remains confined to a relatively narrow plane oriented almost normal to S_{hmin} . In order to create a larger “heat exchanger” volume in the subsurface, a sequence of parallel-trending reservoir disks should be developed by multiple injections at different levels in deviated wells. It is assumed that pre-existing discontinuities strongly determine the reservoir geometry. Hence, additional targets may be identified by massive two- or three-dimensional VSP surveys from existing boreholes.

Acknowledgments

The authors are indebted to Geopower Basel AG for the funding of the entire project. The valuable contributions by the Swiss Seismological Service are gratefully appreciated. In this context we especially thank Nicholas Deichmann for his careful fault plane solution analysis. We appreciate the source parameter estimates by our former colleague Thomas Spillmann (NAGRA) and express our thanks to Hiroshi Asanuma and Yusuke Kumano (Tohoku University) for their contributions with respect to event multiplet analysis. Sincere thanks are given to Reinhard Jung (Jung-Geotherm) and Solexperts AG for their support in the hydraulic characterization of the Basel 1 reservoir. Benoît Valley (Laurentian University) and Keith Evans (Engineering Geology ETH Zürich) are thanked for their help in the characterization of the stress field in Basel 1. Further we would like to thank Angelika Kalt with her team (University of Neuchâtel) and Stefan Schmid (University of Basel) for their contributions regarding the geological characterization of the Basel 1 reservoir. The continuously reliable performance of the network seismometers developed by Peter Malin and his team (University of Auckland) is highly appreciated. Finally, we express our thanks to our paper reviewers for their valuable comments and suggestions.

References

- Ascencio, F., Samaniego, F., Rivera, J., 2006. Application of a spherical-radial heat transfer model to calculate geothermal gradients from measurements in deep boreholes. *Geothermics* 35, 70–78.
- Baer, M., Deichmann, N., Braummiller, J., Clinton, J., Husen, S., Fäh, D., Giardini, D., Kästli, P., Kradofer, U., Wiemer, S., 2007. Earthquakes in Switzerland and surrounding regions during 2006. *Swiss J. Geosci.* 100, 517–528, doi:10.1007/s00015-007-1242-0.
- Bethmann, F., Deichmann, N., Mai, M., 2007. Moment Magnitude. In: Evaluation of the induced seismicity in Basel 2006/2007: locations, magnitudes, focal mechanisms, statistical forecasts and earthquake scenarios. Report of the Swiss Seismological Service to Geopower Basel AG, Switzerland, 152 pp.
- Bommer, J.J., Oates, S., Cepeda, J.M., Lindholm, C., Bird, J., Torres, R., Marroquin, G., Rivas, J., 2006. Control of hazard due to seismicity induced by a hot fractured rock geothermal project. *Eng. Geol.* 83, 287–306.
- Bourdet, D., 2002. Well Test Analysis: The Use of Advanced Interpretation Models. Elsevier, New York, NY, USA, 426 pp.

- Braun, R., 2007. Analyse gebirgsmechanischer Versagenszustände beim Geothermieprojekt Basel. Report to Geopower Basel AG for Swiss Deep Heat Mining Project Basel. Dr. Roland Braun. Consultancy in rock mechanics, Basel, Switzerland, 30 pp.
- Charlez, P.A., 1997. Rock mechanics, vol. 2. Petroleum Applications. Editions Technip, Paris, France, 661 pp.
- Deichmann, N., Ballarin, D., Kastrop, U., 2000. Seismizität der Nord- und Zentralschweiz. Nagra technical report 00-05, Wettingen, Switzerland, 93 pp.
- Deichmann, N., Ernst, J., Wöhlbier, S., 2007a. Data Analysis. In: Evaluation of the Induced Seismicity in Basel 2006/2007: Locations, Magnitudes, Focal Mechanisms, Statistical Forecasts and Earthquake Scenarios. Report of the Swiss Seismological Service to Geopower Basel AG, Basel, Switzerland, 152 pp.
- Deichmann, N., Bachmann, C., 2007b. Data Acquisition. In: Evaluation of the induced seismicity in Basel 2006/2007: locations, magnitudes, focal mechanisms, statistical forecasts and earthquake scenarios. Report of the Swiss Seismological Service to Geopower Basel AG, Basel, Switzerland, 152 pp.
- Dèzes, P., Schmid, S.M., Ziegler, P.A., 2004. Evolution to the European Cenozoic Rift System: interaction of the Alpine and Pyrenean orogens with their foreland lithosphere. *Tectonophysics* 389, 1–33.
- Dyer, B.C., Schanz, U., Spillmann, T., Ladner, F., Häring, M.O., 2008. Microseismic imaging of a geothermal reservoir stimulation. *TLE* 27 (7), 856–869.
- Eshelby, J.D., 1957. The determination of the elastic field of an ellipsoidal inclusion and related problems. *Proc. R. Soc. Lond. A* 241, 376–396.
- Evans, K.F., Roth P., 1998. The state of stress in northern Switzerland inferred from earthquake seismological data and in-situ stress measurements. Report prepared for the Deep Heat Mining (DHM) Project Basel on behalf of Geothermal Explorers Ltd., Pratteln, Switzerland, 26 pp.
- Fjaer, E., Holt, R.M., Horsrud, P., Raaen, A.M., Risnes, R., 1992. Petroleum related rock mechanics. *Developments in Petroleum Science* 33. Elsevier, New York, NY, USA, 338 pp.
- Giardini, D., Wiemer, S., Fäh, D., Deichmann, N., 2004. Seismic Hazard Assessment of Switzerland. Swiss Seimological Service, ETH Zürich, Switzerland, 82 pp.
- Hinsken, S., Ustaszewski, K., Wetzel, A., 2007. Graben width controlling syn-rift sedimentation: the Palaeogene southern Upeer Rhine Graben as an example. *Int. J. Earth Sci. (Geologische Rundschau)* 96, 979–1002.
- Hölker, A., 2005. Ambient noise at potential sites for seismic observation stations of the Deep Heat Mining project Basel. Report prepared for the Deep Heat Mining (DHM) Project Basel on behalf of Geothermal Explorers Ltd., Pratteln, Switzerland, 53 pp.
- Hölker, A., Graf, R., 2005. Modelling the seismograms of micro-seismic events at potential observation stations for the evaluation of alternative observation network configurations. Report prepared for the Deep Heat Mining (DHM) Project Basel on behalf of Geothermal Explorers Ltd., Pratteln, Switzerland, 32 pp.
- Hölker, A., Roth, P., Graf, R., 2005. VSP Survey Otterbach-2. Report for Geothermal Explorers Ltd., Pratteln, Switzerland, 15 pp.
- Kastrop, U., Zoback, M.L., Deichmann, N., Evans, K., Giardini, D., Michael, A.J., 2004. Stress field variations in the Swiss Alps and the northern Alpine foreland derived from inversion of fault plane solutions. *J. Geophys. Res.* 109, B01402, doi:10.1029/2003JB002550.
- Käser, B., Kalt, A., Borel, J., 2007. The crystalline basement drilled at the Basel-1 geothermal site. A preliminary petrological-geochemical study. Report to Geopower Basel AG for Swiss Deep Heat Mining Project Basel. Institut de Géologie et d'Hydrogéologie, Université de Neuchâtel, Switzerland, 84 pp.
- Kumano, Y., Asanuma, H., Hotta, A., Niitsuma, H., Schanz, U., Häring, M., 2007. Reservoir structure delineation by microseismic multiplet analysis at Basel, Switzerland, 2006. Paper presented at the 77th SEG meeting, San Antonio, TX, USA, Extended Abstracts, pp. 1271–1276.
- Jung, R., Ortiz, A., 2007. Analyse eines hydraulischen Injektionstests und eines massiven Wasserfrac-Tests in der Geothermiebohrung Basel-1. Institut für Geowissenschaftliche Gemeinschaftsaufgaben Hannover (Germany) report to Geopower Basel AG for the Swiss Deep Heat Mining Project Basel, 20 pp.
- Laubscher, H., 2001. Plate interactions at the southern end of the Rhine graben. *Tectonophysics* 343, 1–19.
- Ljunggren, C., Chang, Y., Janson, T., Christiansson, R., 2003. An overview of rock stress measurement methods. *Int. J. Rock Mech. Mining Sci.* 40, 975–989.
- Madariaga, R., 1976. Dynamics of an expanding circular fault. *Bull. Seismol. Soc. Am.* 66, 639–666.
- Plenefisch, T., Bonjer, K.-P., 1997. The stress field in the Rhine Graben area inferred from earthquake focal mechanisms and estimation of frictional parameters. *Tectonophysics* 275, 71–97.
- Reinecker, J., Heidbach, O., Tingay, M., Sperner, B., Müller, B., 2005. The release 2005 of the World Stress Map. (available online at www.world-stress-map.org).

- Roux, B., Sanyal, S.K., Brown, S., 1980. An improved approach to estimating true reservoir temperature from transient temperature data. In: Paper 8888 presented at the 1980 SPE California Regional Meeting, Los Angeles, CA, USA, pp. 373–384.
- Rutishauser, 2006. Erschütterungstechnische Beratung. Ingenieurbüro für Bau, Verkehr und Umwelt GmbH, Zürich report prepared for Geopower Basel AG for Swiss Deep Heat Mining Project Basel. 5121/01/AE/RU, Basel, Switzerland, 22 pp.
- Rutqvist, J., Stephansson, O., 2003. The role of hydromechanical coupling in fractured rock engineering. *Hydrogeol. J.* 11, 7–40.
- Schorlemmer, D., Wiemer, S., Wyss, M., 2005. Variations in earthquake-size distribution across different stress regimes. *Nature* 437, 539–542.
- Ustazewski, K., Schmid, S.M., 2007. Latest Pliocene to recent thick-skinned tectonics at the Upper Rhine Graben–Jura Mountains junction. *Swiss J. Geosci.* 100 (2), 293–312.
- Valley, B., Evans, K.F., 2006. Stress orientation at the Basel geothermal site from wellbore failure analysis in BS1. Report to Geopower Basel AG for Swiss Deep Heat Mining Project Basel. ETH Report Nr.: ETH 3465/56. Ingenieurgeologie ETH Zürich, Switzerland, 29 pp.
- Wiemer, S., Bachmann, C., Woessner, J., 2007. Statistical Analysis and Earthquake Probabilities. In: Evaluation of the induced Seismicity in Basel 2006/2007: Locations, Magnitudes, Focal Mechanisms, Statistical Forecasts and Earthquake Scenarios. Report of the Swiss Seismological Service to Geopower Basel AG, Basel, Switzerland, 152 pp.
- Zoback, M.D., 2007. *Reservoir Geomechanics*. Cambridge University Press, New York, NY, USA, 449 p.